Applied Physics Letters

RESEARCH ARTICLE | JUNE 23 2026

Full-color imaging diffractive lenses fabricated by two-photon lithography

Rodion S. Chetverin ; Margarita I. Sharipova ; Andrey A. Fedyanin

Appl. Phys. Lett. 128, 251103 (2026)
https://doi.org/10.1063/5.0335254

AIP Publishing

Applied Physics Letters ARTICLE pubs.aip.org/aip/apl

Full-color imaging diffractive lenses fabricated by two-photon lithography

Cite as: Appl. Phys. Lett. **128**, 251103 (2026); doi: 10.1063/5.0335254
Submitted: 23 March 2026 · Accepted: 3 June 2026 ·
Published Online: 23 June 2026

Rodion S. Chetverin, Margarita I. Sharipova, and Andrey A. Fedyanin[a)]

AFFILIATIONS

Faculty of Physics, Lomonosov Moscow State University, Moscow, Russia

[a)]Author to whom correspondence should be addressed: fedyanin@nanolab.phys.msu.ru

ABSTRACT

Diffractive lenses allow bulky refractive optical elements to be replaced by compact solutions, making them essential for miniaturized optical systems. However, diffractive lenses suffer from strong chromatic aberrations, which severely limit their applicability in imaging systems operating over a finite spectral bandwidth, such as the visible spectrum. We employed two-photon lithography to achieve full-color imaging in diffractive lenses with an engineered phase profile incorporating a third-order nonlinear term.

Two-photon laser lithography (TPL) is a rapidly developing technique for fabricating planar and three-dimensional polymer structures with spatial resolution down to 100 nm.[1] The feasibility of using this method to produce microlenses for the visible[2,3] and x-ray spectral ranges[4,5] together with other microsized optical elements[6,7] has recently been demonstrated. In addition to printing single optical elements, TPL enables the fabrication of compound optical systems—such as microlens arrays[8] and objective lenses[9]—in a single manufacturing cycle, as well as the printing of micro-optical elements directly on various substrates, such as optical fibers,[10] photonic crystals,[11] silicon wafers,[12] CMOS sensors,[13] and membranes.[14]

Diffractive optical elements (DOEs) are of particular interest due to their ability to specify an arbitrary amplitude or phase profile, along with their compactness, allowing their use in a wide range of applications from laser processing and micro/nanolithography to adaptive optics, holography, and telecommunications.[15] Examples of diffractive optical elements include planar focusing optics such as Fresnel zone plates, which consist of an array of alternating transparent and opaque concentric rings,[16] and Fresnel lenses, in which the height of the concentric rings varies continuously.[17] Such elements may have heights smaller than or comparable to the optical wavelength.

However, diffractive lenses inherently suffer from large chromatic aberrations, manifested as a strong dependence of the focal length on the wavelength. These chromatic aberrations arise from phase discontinuities at the zone boundaries[18] and, as a result, make DOEs unsuitable for broadband imaging.

Various methods have been proposed to produce achromatic diffractive lenses.[19] First, several optical components, such as refractive and diffractive lenses, can be combined to overcome chromatic dispersion. This approach is referred to as a hybrid lens design when components of different physical nature are used,[20] or as a multi-lens or multi-layer system when several DOEs are stacked to achieve an achromatic response.[21,22] The obvious drawback of this approach is its design complexity, which requires multiple optical surfaces instead of a single-element design.

The second solution is a multi-material strategy, when using several materials with different dispersion in one DOE allows one to control group delay and group delay dispersion to compensate for chromatic aberration in the desired waverange.[23] This composite-DOE method is a more sophisticated variation of the multi-lens or multi-layer approach, as it typically involves several optical surfaces combined into a sandwich structure.[24,25]

Other methods attempt to optimize the structure for several target wavelengths, either by inverse design,[26] by engineering phase discontinuities at the zone boundaries (e.g., harmonic DOE[27]) or by dividing the lens into multiple zones, each designed for a specific wavelength. The resulting DOE is therefore polychromatic rather than truly achromatic, providing similar focusing only for a predetermined discrete set of wavelengths. Achromatic lenses for broadband spectra have also been demonstrated recently, using optimization methods.[28,29]

An alternative approach to correct chromatic aberrations is to increase the depth of focus (DOF) of the system. This method reduces the impact of chromatic aberrations by making the system less sensitive to focal shifts at different wavelengths. When the depth of focus is large, the image remains sufficiently sharp over a considerable distance along the optical axis for each spectral component. This leads to partial overlap of focal regions corresponding to different colors and reduces the visibility of longitudinal chromatic aberration, thus improving color uniformity and overall image quality without complex optical correction.[30]

In recent years, rapid advances in additive technologies have significantly accelerated the development of complex-shaped optical elements.[31–34] One of the additive manufacturing techniques, two-photon lithography, enables the maskless three-dimensional fabrication of freeform microstructures through localized photopolymerization induced by two-photon absorption.[35]

The present work is devoted to the design, fabrication by two-photon laser lithography, and optical characterization of diffractive lenses with an extended depth of focus, as well as their comparison with conventional Fresnel lenses.

The focal length of diffractive lenses is inversely dependent on the wavelength.[36] For an optical system, this implies that image plane blur differs for different spectral components of the source. Increasing the depth of focus makes the system insensitive to chromatic shifts of the focal plane, since the focal spot is elongated along the optical axis. However, this also leads to a reduction in the signal-to-noise ratio, since light is distributed over a larger volume.[37]

The depth of focus can be increased by adding a cubic term to the lens phase profile.[38] The cubic term breaks the radial symmetry of the lens and introduces a continuously varying phase gradient across the aperture; therefore, various regions of the pupil redirect light in different directions, which results in extended depth of focus. In this case, the phase profile of the lens takes the following form:[37]

$$\phi(x, y) = \frac{2\pi}{\lambda_0}\left(\sqrt{x^2 + y^2 + f^2} - f\right) + \frac{\alpha}{L^3}\left(x^3 + y^3\right), \quad (1)$$

where x and y are the coordinates in the lens plane, f is the focal length, λ_0 is the operating wavelength, α is the cubic phase function coefficient, and L is half the lens aperture width. The phase profile of a planar DOE lens can be obtained from Eq. (1) by constraining the phase ϕ to the limited modulation range, usually $[0, 2\pi]$.[39]

If $\alpha = 0$, Eq. (1) describes the profile of a conventional hyperbolic lens. The relationship between the phase profile $\phi(x, y)$ and the lens height $h(x, y)$ at an arbitrary point is described by[29]

$$\phi(x, y) = \frac{2\pi}{\lambda_0}(n - 1)h(x, y), \quad (2)$$

where n is the refractive index of the lens material at wavelength λ_0.

Figure 1 illustrates the variation in lens profile and optical response with changing cubic coefficient α.

To select the optimal cubic coefficient, numerical calculations were performed using the FDTD method for several α values in the range of 0–100π (see supplementary material S7 for more details about numerical simulations). For all lenses, the following parameters were chosen: central wavelength $\lambda_0 = 500$ nm, focal length $f = 100\,\mu$m, aperture $100\,\mu$m, and refractive index $n = 1.5$, which approximately corresponds to the value reported in the literature for the SZ2080 photoresist in the visible range.[40] The height profiles of the lenses with various values of cubic coefficient α are shown in Fig. 1(c) on the top, and the cross sections of the profiles in the diagonal direction are shown on the bottom. Figure 1(b) displays the

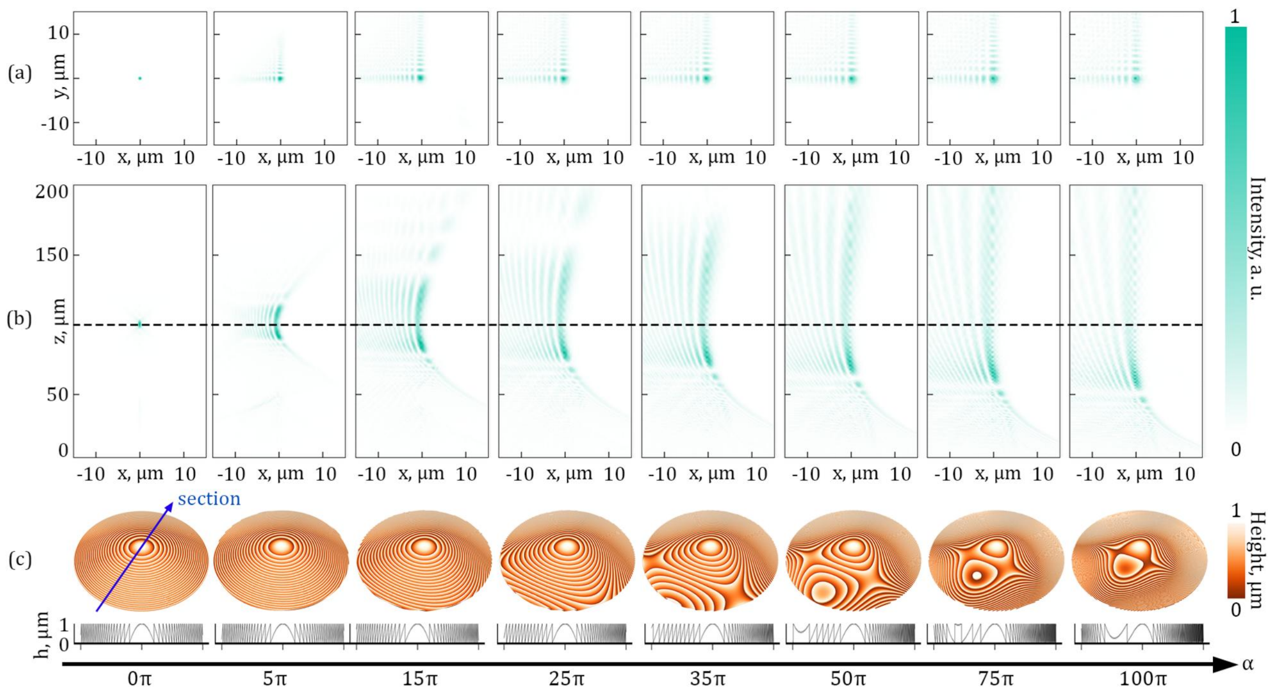

FIG. 1. Intensity distributions in the focal plane $z = 100\,\mu m$ (a) and along the optical axis (b), and planar hyperbolic lenses' height profiles and cross sections (c) for the wavelength of 500 nm with changing cubic coefficient α from 0 to 100π (left to right).

intensity distributions of light propagating after the lens. The wavelength of light is $\lambda = 500$ nm, equal to the design wavelength of the lens λ_0. The intensity distributions were also calculated for three other wavelengths: 400, 550, and 700 nm (see supplementary material Fig. 3). Figure 1(a) shows the point spread function (PSF) in the image plane of the optical system, which is $z = 100\,\mu$m. For $\alpha = 0$, the lens height profile is radially symmetric, and the focal spot is tightly focused in a small volume in the x, y, and z directions. When α begins to grow, the height profile starts to become asymmetric, and the focal spot stretches in the z direction. As for the image plane, the PSF becomes asymmetric, with pronounced secondary peaks forming two tails positioned at a normal angle to each other. As the cubic coefficient α increases further, the region with the maximum intensity in the focal point moves closer to the lens and elongates further along the optical axis. This behavior is illustrated in Fig. 1(b). Radiation is distributed over a larger volume, which reduces the peak intensity value in the focal spot. Therefore, one should carefully choose the value of the cubic coefficient α to balance between the desired effect of extended depth of focus (EDOF) to achieve focusing overlap throughout the visible region and the tolerable decrease in focusing efficiency.

Figure 2(a) shows the calculated focal spot length vs the cubic coefficient value α for three central wavelengths, 700, 550, and 400 nm, which are beginning, middle, and end points in the visible wavelength region and roughly correspond to the red, green, and blue (RGB) colors. Here, we define the focal spot longitudinal size as the axial interval over which the light intensity is not less than 0.25 of the maximum. Rather than relying on standard image-quality criteria such as Rayleigh length or circle of confusion, we adopt a relative-intensity threshold that is simple to measure and reproduce across experiments, and therefore this metric can serve as a useful, industry-applicable benchmark for comparing different lens designs. For $\alpha = 0$, no overlap is observed in the focal spots for the three colors. The focal ranges for RGB colors are 66–71, 87–93, and 124–131 μm, respectively. With a small non-zero α, the focal spot size begins to elongate in the light propagation direction, resulting in EDOF. The focal spot length extension rate with increasing α is the smallest for the red color and the largest for the blue color. The growth is asymmetrical: the left branches, designating shorter focal distances, extend steadily to even shorter distances across all range of α; the right branches, which show longer end of focal distances, grow faster with α than the left branches. However, the growth of the right branches stops abruptly at some point—the exact position varies with color, $\alpha = 50\pi, 25\pi, 15\pi$ for RGB colors, respectively—and then the focal spot distance decreases. This behavior can be explained by the shift of peak intensity in the focal spot to the shorter distances, resulting in the rapid intensity drop at the far end of the focal spot. The minimal value of α with overlap is close to 20π, where all focal points meet within the range along the optical axis of 3 μm, from 97 to 100 μm. For $\alpha = 25\pi$, the focal points for the RGB colors overlap within the larger range of 12 μm: from 93 to 105 μm. The longest overlap range is observed at $\alpha \simeq 30\pi$. For $35\pi < \alpha < 55\pi$, the overlap range remains roughly the same and gradually shifts to shorter distances. After that, the overlap range value rapidly decreases. For $\alpha = 60\pi$, the RGB focal spot overlap disappears. This is because even though the entire intensity is distributed over a larger area, the high-intensity region of the focal spot decreases with increasing α. In summary, the values of the cubic coefficient α with the overlap of focal points are within the range of $[20\pi, 55\pi]$.

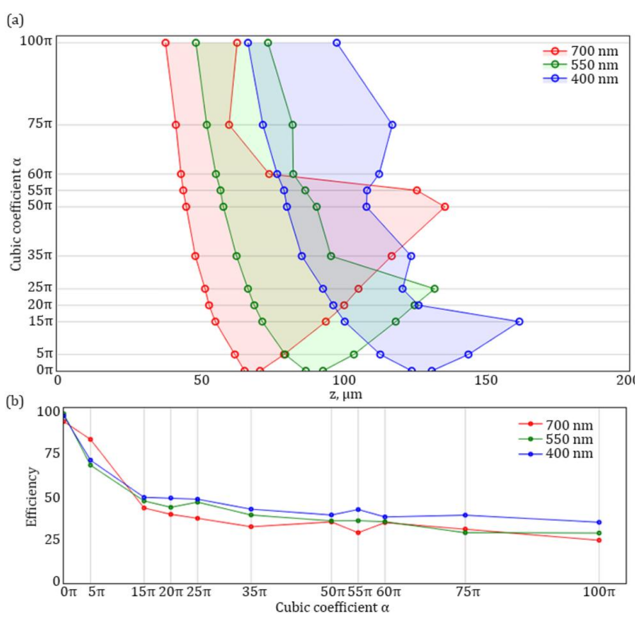

FIG. 2. Depth of focus (a) and efficiency (b) for red, green, and blue light.

Figure 2(b) demonstrates another important characteristic of the lens, relative focusing efficiency, calculated here as the ratio of energy within 3× the full widths at half maximum (FWHM) of the spot to the total energy in a focal plane section[41] along the x-axis (see supplementary material S6). As can be seen, the efficiency value gradually decreases with α. Therefore, when considering efficiency, the lowest values of the cubic coefficient α are preferable. Thus, the optimal value of α for an EDOF lens is the minimal α at which the focal points of all wavelengths within the range considered (400–700 nm) overlap, that is, $\alpha = 20\pi$ in our case. However, we have chosen the cubic coefficient value $\alpha = 25\pi$ for further experiments with an almost the same calculated efficiency value and a longer overlap region.

Figure 3 shows the calculated intensity distributions along the optical axis, in the focal planes of each color for conventional ($\alpha = 0$), and distribution at the common focal plane $z = 100\,\mu$m for EDOF ($\alpha = 25\pi$) diffractive lenses. For a conventional Fresnel lens without a cubic term, i.e., $\alpha = 0$, the focal volume is limited to 5.5–7 μm, depending on the wavelength, while the RGB positions of focal spots are spaced by a considerable distance of about 60 μm [Fig. 3(a)]. As can be seen in Fig. 3(b), for this case, the focal spots in the image plane are small circles with an FWHM of about 0.7 μm. In contrast, for the cubic term $\alpha = 25\pi$ we observe an asymmetric PSF [Fig. 3(d)]. The focal region consists of multiple intensity maxima confined to a single quadrant, with the intensity decreasing away from the optical axis due to the cubic phase modulation. As for the intensity distribution along the optical axis [Fig. 3(c)], for the EDOF lens the focal volume is distributed over a considerable distance along the optical axis—with an estimated depth of focus of 28 μm for 550 nm, and 90 μm, 32 μm and for RGB colors, respectively. The RGB focal volumes overlap in the axial range from 93 to 105 μm. As the designed focal distance was longer, $f = 100\,\mu$m, we notice that the focal spot shifts toward shorter distances.

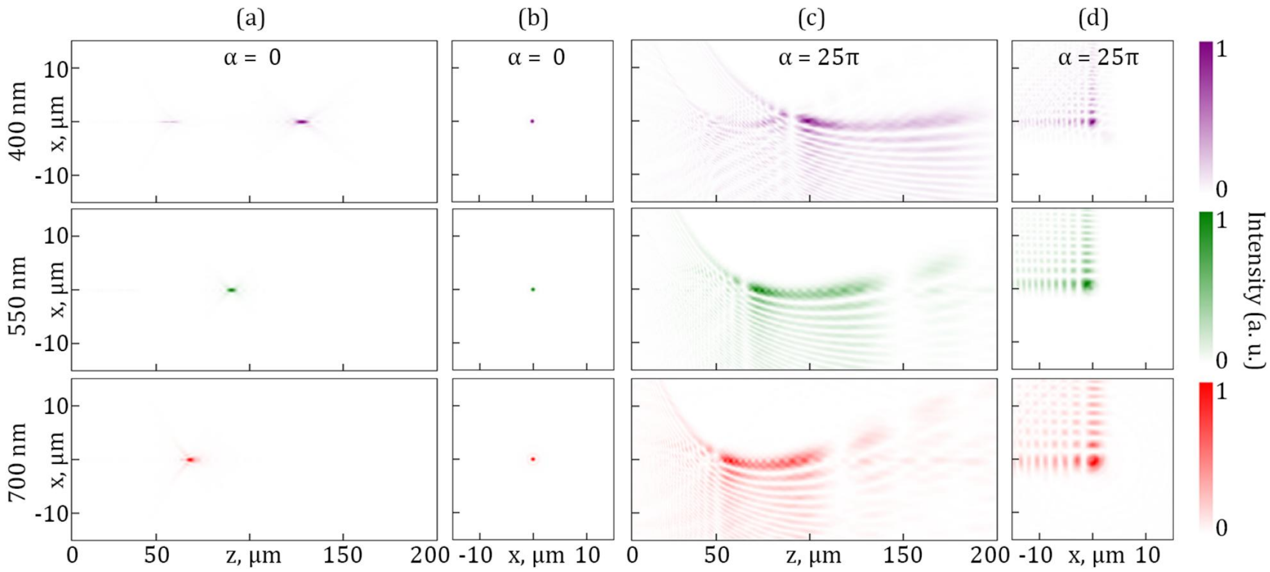

FIG. 3. Simulated intensity distribution along the optical axis (a) and (c) and the focal planes (b) and (d) for 400 nm (top), 550 nm (middle), and 700 nm (bottom) for the lenses with $\alpha = 0$ (a) and (b) and $\alpha = 25\pi$ (c) and (d).

The SZ2080 photoresist was used as a printing material, having a refractive index ranging from 1.447 to 1.554 in the visible spectral range.[40,42] The liquid resist was applied onto a pre-cleaned glass substrate, and then baked on a hot plate at 80 °C for one hour to solidify the resist. The prepared substrates were then exposed to laser radiation during a printing process in a custom-built TPL setup[43] (see supplementary material S1). After printing, the unexposed resist was removed using methyl isobutyl ketone.

We have fabricated samples with $\alpha = 0$, 25π, 35π, and 50π. The print model was set in the form of a list of points in cylindrical coordinates. The distance between the points in the radial direction and along the circumference is 0.2 μm. All samples were produced at a power of 8 mW and an exposure time of 1 ms per point. SEM images of the fabricated lenses and the corresponding height profile models are shown in Fig. 4. Apart from minor surface debris and occasional protrusions, the fabricated samples exhibit high structural fidelity, and the height profile of the fabricated samples agrees well with the target model (see supplementary material S4 for more pictures), which is also confirmed by measurements with an atomic force microscope (see supplementary material S5).

Figure 5 shows the measured field distributions along the optical axis and in the focal planes. Experimental measurements of the focusing properties of the fabricated samples were performed using a supercontinuum laser source in the 550–700 nm range and a 405 nm diode laser (see supplementary material S2 for the experimental schematic). For a conventional lens with $\alpha = 0$, the expected wavelength-dependent focal distances are clearly visible; the focal spots of blue, green, and red colors are spread along the optical axis at a significant distance and do not intersect. The EDOF lens with a cubic coefficient $\alpha = 25\pi$ indeed exhibits an extended depth of focus; as a result, at a distance of 67–92 μm, all colors overlap, and full-color focusing is achieved. The experimental results qualitatively agree with the optical simulations shown in Fig. 3. However, the measured focal distance is positioned closer to the lens and is two times wider: 25 μm compared to expected 12 μm. We explain this by the more moderate intensity variation inside the focal spot in the longitudinal direction observed in the experiment, which results in a larger focal spot longitudinal size. The shift to shorter distances in the experiment is probably caused by wavelength mismatch; the discrepancy with numerical simulations can be attributed to a slight difference between the wavelength value for the blue color (400 nm in simulations and 405 nm in the experiment).

The transmittance, FWHM, and relative focusing efficiency of the manufactured samples were also measured (see supplementary material S6) for blue, green, and red light, respectively. The average transmittance was 0.70 for a standard Fresnel lens, and 0.66 for the EDOF lens. The relative focusing efficiency (defined in the same fashion as

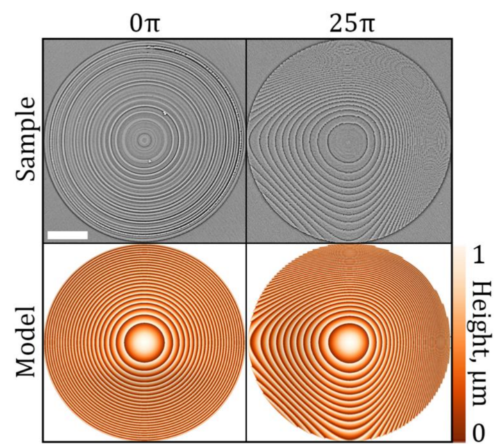

FIG. 4. SEM images of the fabricated lenses (top) and their corresponding models (bottom) with $\alpha = 0$ (left) and $\alpha = 25\pi$ (right). The scale bar corresponds to 20 μm.

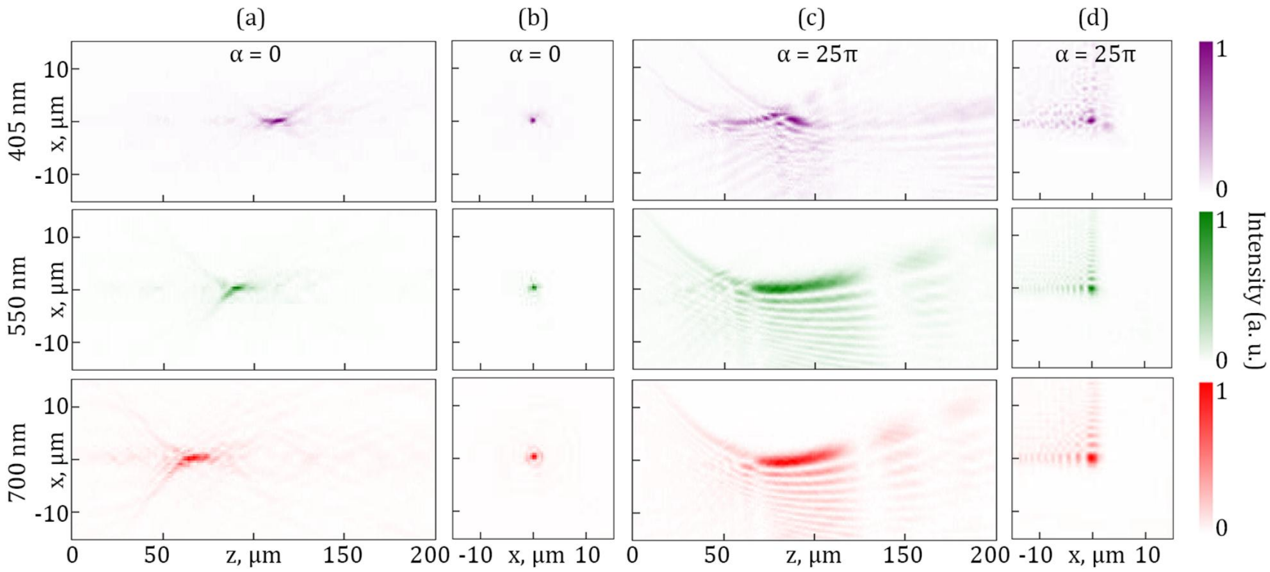

FIG. 5. Measured intensity distribution along the optical axis (a), (c) and the focal planes (b), (d) for 405 nm (top), 550 nm (middle), and 700 nm (bottom) for the lenses with $\alpha = 0$ and $\alpha = 25\pi$, respectively.

earlier for numerical simulation) of an achromatic lens with $\alpha = 25\pi$ is 42%–46%, while for a conventional lens, the observed efficiency is 47%–60% (see supplementary material S6). Thus, it is shown that the lenses allow for full-color focusing without a significant loss of efficiency or resolution. The imaging tests have also been performed on fabricated samples using broadband illumination, see supplementary material S8. While for the lens with $\alpha = 25\pi$ the image is more blurred compared to the one with $\alpha = 0$, figures of different color remain in focus due to extended depth of field.

In conclusion, we have realized a simple and robust approach to make full-color planar diffractive lenses. This method uses wavefront coding with a cubic phase term and is easy to fabricate. Numerical calculations find that a medium cubic nonlinearity balances chromatic focal overlap and focusing well, giving broadband focal-volume intersection across the visible spectrum. We made these lenses using two-photon laser lithography in a single-layer polymer structure, achieving sub-micrometer relief and faithful reproduction of the designed phase profile. Measurements support the simulations, with observed extended depth of focus and spectral overlap of the focal regions from 405 to 700 nm, without greatly sacrificing focusing performance. This approach allows for compact, single-element achromatic micro-optics without the need for multi-layer or multi-material designs. It works well for integration into small imaging systems, fiber-end optics, and photonic platforms.

See the supplementary material for schematics of the optical characterization and TPL fabrication setups, measured axial intensity distributions, SEM images of all lenses, atomic force microscopy results for $\alpha = 0\pi$ and $\alpha = 25\pi$ lenses, and measured characteristics of the fabricated lenses.

The authors thank Alexander Yu. Frolov for the atomic force microscopy measurements and Sofya K. Yurovskaya for help with the experimental setup. This research was performed using equipment provided by the MSU Development Program. The study was financially supported by a grant of the Russian Science Foundation (No. 25-12-00355), https://rscf.ru/project/25-12-00355/.

AUTHOR DECLARATIONS

Conflict of Interest

The authors have no conflicts to disclose.

Author Contributions

Rodion S. Chetverin: Conceptualization (equal); Data curation (equal); Investigation (equal); Methodology (equal); Validation (equal); Writing – original draft (equal). **Margarita I. Sharipova:** Conceptualization (equal); Data curation (equal); Formal analysis (equal); Investigation (equal); Methodology (equal); Validation (equal); Writing – original draft (equal). **Andrey A. Fedyanin:** Conceptualization (equal); Funding acquisition (equal); Project administration (equal); Supervision (equal); Writing – review & editing (equal).

DATA AVAILABILITY

The data that support the findings of this study are available from the corresponding author upon reasonable request.

REFERENCES

[1]J.-F. Xing, X.-Z. Dong, W.-Q. Chen, X.-M. Duan, N. Takeyasu, T. Tanaka, and S. Kawata, "Improving spatial resolution of two-photon microfabrication by using photoinitiator with high initiating efficiency," Appl. Phys. Lett. **90**, 131106 (2007).

[2]R. Guo, S. Xiao, X. Zhai, J. Li, A. Xia, and W. Huang, "Micro lens fabrication by means of femtosecond two photon photopolymerization," Opt. Express **14**, 810–816 (2006).

[3]B. Du, H. Zhang, J. Xia, J. Wu, H. Ding, and G. Tong, "Super-resolution imaging with direct laser writing-printed microstructures," J. Phys. Chem. A **124**, 7211–7216 (2020).
[4]D. Qu, S. Zhao, P. Qi, A. Bergamaschi, M. R. D. Veeraraj, R. Dinapoli, J. Heymes, J. Vila-Comamala, and C. David, "Achromatic laboratory full-field transmission x-ray microscope," Photonics Res. **14**, 392–400 (2026).
[5]M. I. Sharipova, T. G. Baluyan, K. A. Abrashitova, G. E. Kulagin, A. K. Petrov, A. S. Chizhov, T. B. Shatalova, D. Chubich, D. A. Kolymagin, A. G. Vitukhnovsky, V. O. Bessonov, and A. A. Fedyanin, "Effect of pyrolysis on microstructures made of various photoresists by two-photon polymerization: Comparative study," Opt. Mater. Express **11**, 371–384 (2021).
[6]H. Wang, C.-F. Pan, C. Li, K. S. Menghrajani, M. A. Schmidt, A. Li, F. Fan, Y. Zhou, W. Zhang, H. Wang *et al.*, "Two-photon polymerization lithography for imaging optics," Int. J. Extrem. Manuf. **6**, 042002 (2024).
[7]K. R. Safronov, V. O. Bessonov, D. V. Akhremenkov, M. A. Sirotin, M. N. Romodina, E. V. Lyubin, I. V. Soboleva, and A. A. Fedyanin, "Miniature Otto prism coupler for integrated photonics," Laser Photonics Rev. **16**, 2100542 (2022).
[8]A. K. Petrov, V. O. Bessonov, K. A. Abrashitova, N. G. Kokareva, K. R. Safronov, A. A. Barannikov, P. A. Ershov, N. B. Klimova, I. I. Lyatun, V. A. Yunkin, M. Polikarpov, I. Snigireva, A. A. Fedyanin, and A. Snigirev, "Polymer X-ray refractive nano-lenses fabricated by additive technology," Opt. Express **25**, 14173–14181 (2017).
[9]T. Gissibl, S. Thiele, A. Herkommer, and H. Giessen, "Two-photon direct laser writing of ultracompact multi-lens objectives," Nat. Photonics **10**, 554–560 (2016).
[10]C. Liberale, G. Cojoc, P. Candeloro, G. Das, F. Gentile, F. De Angelis, and E. Di Fabrizio, "Micro-optics fabrication on top of optical fibers using two-photon lithography," IEEE Photonics Technol. Lett. **22**, 474–476 (2010).
[11]K. R. Safronov, D. N. Gulkin, I. M. Antropov, K. A. Abrashitova, V. O. Bessonov, and A. A. Fedyanin, "Multimode interference of Bloch surface electromagnetic waves," ACS Nano **14**, 10428–10437 (2020).
[12]I. Katsantonis, M. Manousidaki, A. D. Koulouklidis, C. Daskalaki, I. Spanos, C. Kerantzopoulos, A. C. Tasolamprou, C. M. Soukoulis, E. N. Economou, S. Tzortzakis *et al.*, "Strong and broadband pure optical activity in 3D printed THz chiral metamaterials," Adv. Opt. Mater. **11**, 2300238 (2023).
[13]S. Thiele, K. Arzenbacher, T. Gissibl, H. Giessen, and A. M. Herkommer, "3D-printed eagle eye: Compound microlens system for foveated imaging," Sci. Adv. **3**, e1602655 (2017).
[14]D. M. Zhigunov, M. I. Sharipova, Y. G. Gladush, D. V. Krasnikov, V. O. Bessonov, A. A. Fedyanin, and A. G. Nasibulin, "Single-walled carbon nanotube pristine films: Thickness determination, antireflective properties and two-photon 3D lithography demonstration," Opt. Mater. **167**, 117289 (2025).
[15]S. N. Khonina, N. L. Kazanskiy, R. V. Skidanov, and M. A. Butt, "Advancements and applications of diffractive optical elements in contemporary optics: A comprehensive overview," Adv. Mater. Technol. **10**, 2401028 (2024).
[16]K. Rastani, A. Marrakchi, S. F. Habiby, W. M. Hubbard, H. Gilchrist, and R. E. Nahory, "Binary phase Fresnel lenses for generation of two-dimensional beam arrays," Appl. Opt. **30**, 1347–1354 (1991).
[17]M. Haruna, M. Takahashi, K. Wakahayashi, and H. Nishihara, "Laser beam lithographed micro-Fresnel lenses," Appl. Opt. **29**, 5120–5126 (1990).
[18]E. Arbabi, A. Arbabi, S. M. Kamali, Y. Horie, and A. Faraon, "Multiwavelength polarization-insensitive lenses based on dielectric metasurfaces with meta-molecules," Optica **3**, 628–633 (2016).
[19]C. Peng, J. Yao, and D. P. Tsai, "Progress in metalenses: From single to array," Opto-Electron. Technol. **1**, 250004 (2025).
[20]V. V. Evdokimova, V. V. Podlipnov, N. A. Ivliev, M. V. Petrov, S. V. Ganchevskaya, V. A. Fursov, Y. Yuzifovich, S. O. Stepanenko, N. L. Kazanskiy, A. V. Nikonorov, and R. V. Skidanov, "Hybrid refractive-diffractive lens with reduced chromatic and geometric aberrations and learned image reconstruction," Sensors **23**, 415 (2022).
[21]C.-F. Pan, H. Wang, H. Wang, P. N. S. Q. Ruan, S. Wredh, Y. Ke, J. Y. E. Chan, W. Zhang, C.-W. Qiu *et al.*, "3D-printed multilayer structures for high-numerical aperture achromatic metalenses," Sci. Adv. **9**, eadj9262 (2023).
[22]S. Thiele, C. Pruss, A. M. Herkommer, and H. Giessen, "3D printed stacked diffractive microlenses," Opt. Express **27**, 35621–35630 (2019).
[23]D. Werdehausen, S. Burger, I. Staude, T. Pertsch, and M. Decker, "Dispersion-engineered nanocomposites enable achromatic diffractive optical elements," Optica **6**, 1031–1038 (2019).
[24]G. Vallerotto, M. Victoria, S. Askins, R. Herrero, C. Domínguez, I. Antón, and G. Sala, "Design and modeling of a cost-effective achromatic Fresnel lens for concentrating photovoltaics," Opt. Express **24**, A1245–A1256 (2016).
[25]S. M. Ebstein, "Achromatic diffractive optical elements," Proc. SPIE **2404**, 211–216 (1995).
[26]M. Choi, J. Kim, S. Moon, K. Shin, S.-W. Nam, Y. Park, D. Kang, G. Jeon, K-i Lee, D. H. Yoon *et al.*, "Roll-to-plate printable RGB achromatic metalens for wide-field-of-view holographic near-eye displays," Nat. Mater. **24**, 535–543 (2025).
[27]Y. Zheng, J. Du, B. Lei, J. Bian, L. Wang, and B. Fan, "Design, analysis, and manufacturing of diffractive achromatic optical systems," Micromachines **16**, 322 (2025).
[28]X. Xiao, Y. Zhao, X. Ye, C. Chen, X. Lu, Y. Rong, J. Deng, G. Li, S. Zhu, and T. Li, "Large-scale achromatic flat lens by light frequency-domain coherence optimization," Light: Sci. Appl. **11**, 323 (2022).
[29]Y. Chu, X. Li, X. Xiao, S. Zhu, and T. Li, "Achromatic multi-level diffractive lenses and related applications," Adv. Phys. X **10**, 2580626 (2025).
[30]Y. Huang, M. Xiong, P. Zhang, C. Zhu, B. Cui, X. Zhao, Y. Qiu, S. Zheng, Y. Dong, Q. Zhong, and T. Hu, "Broadband achromatic metalens with enhanced field of view for thermal image," J. Lightwave Technol. **43**, 3397–3403 (2025).
[31]M. Vaezi, H. Seitz, and S. Yang, "A review on 3D micro-additive manufacturing technologies," Int. J. Adv. Manuf. Technol. **67**, 1721–1754 (2013).
[32]P. Somers, A. Münchinger, S. Maruo, C. Moser, X. Xu, and M. Wegener, "The physics of 3D printing with light," Nat. Rev. Phys. **6**, 99–113 (2023).
[33]M. H. Eisa, A. Zia, Z. Hassan, and S. Saeed, "Ultrafast laser two-photon lithography for metasurface engineering: Advances in fabrication and photonic applications," Laser Photonics Rev. **20**, e02914 (2026).
[34]C. Jiang, M. Gu, H. Feng, Y. Tian, and X. Jing, "3D printing technologies for metasurface fabrication and applications of metasurfaces manufactured by 3D printing processes," J. Appl. Phys. **139**, 080701 (2026).
[35]M. Farsari and B. N. Chichkov, "Two-photon fabrication," Nat. Photonics **3**, 450–452 (2009).
[36]P. Wang, N. Mohammad, and R. Menon, "Chromatic-aberration-corrected diffractive lenses for ultra-broadband focusing," Sci. Rep. **6**, 21545 (2016).
[37]S. Colburn, A. Zhan, and A. Majumdar, "Metasurface optics for full-color computational imaging," Sci. Adv. **4**, eaar2114 (2018).
[38]H. B. Wach, E. R. Dowski, and W. T. Cathey, "Control of chromatic focal shift through wave-front coding," Appl. Opt. **37**, 5359–5367 (1998).
[39]J.-G. Yun, H. Kang, K. Lee, Y. Jeong, E. Lee, J. Kim, M. Choi, B. Koo, D. Kim, J. Choi *et al.*, "Compact eye camera with two-third wavelength phase-delay metalens," Nat. Commun. **16**, 7299 (2025).
[40]A. Žukauskas, G. Batavičiūtė, M. Ščiuka, Z. Balevičius, A. Melninkaitis, and M. Malinauskas, "Effect of the photoinitiator presence and exposure conditions on laser-induced damage threshold of ORMOSIL (SZ2080)," Opt. Mater. **39**, 224–231 (2015).
[41]Y. Zheng, M. Xu, M. Pu, F. Zhang, D. Sang, Y. Guo, X. Li, X. Ma, and X. Luo, "Designing high-efficiency extended depth-of-focus metalens via topology-shape optimization," Nanophotonics **11**, 2967–2975 (2022).
[42]A. Ovsianikov, J. Viertl, B. Chichkov, M. Oubaha, B. MacCraith, I. Sakellari, A. Giakoumaki, D. Gray, M. Vamvakaki, M. Farsari *et al.*, "Ultra-low shrinkage hybrid photosensitive material for two-photon polymerization microfabrication," ACS Nano **2**, 2257–2262 (2008).
[43]M. D. Aparin, T. G. Baluyan, M. I. Sharipova, M. A. Sirotin, E. V. Lyubin, I. V. Soboleva, V. O. Bessonov, and A. A. Fedyanin, "Fabrication of optical microstructures with gradient refractive index by two-photon laser lithography," Bull. Russ. Acad. Sci. Phys. **87**, 710–714 (2023).